

# Robust extended states in Anderson model on partially disordered random regular graphs

Daniil Kochergin<sup>1,2</sup>, Ivan M. Khaymovich<sup>3,4,\*</sup>, Olga Valba<sup>5,2</sup>, and Alexander Gorsky<sup>6,2</sup>

**1** Moscow Institute of Physics and Technology, Dolgoprudny 141700, Russia

**2** Laboratory of Complex Networks, Center for Neurophysics and Neuromorphic Technologies, Moscow, Russia

**3** Nordita, Stockholm University and KTH Royal Institute of Technology Hannes Alfvéns väg 12, SE-106 91 Stockholm, Sweden

**4** Institute for Physics of Microstructures, Russian Academy of Sciences, 603950 Nizhny Novgorod, GSP-105, Russia

**5** Higher School of Economics, Moscow, Russia

**6** Institute for Information Transmission Problems, Moscow 127994, Russia

\* ivan.khaymovich@gmail.com

September 13, 2023

## Abstract

In this work we analytically explain the origin of the mobility edge in partially disordered ensemble of random regular graphs (RRG), with the connectivity  $d$ , the position of which is under control. It is shown that the mobility edge in the spectrum survives in some region in  $(\beta, d)$ -parameter plane at infinitely large uniformly distributed disorder, where  $\beta$  stands for the fraction of disordered nodes. The critical curve separating extended and localized states is derived analytically and confirmed numerically. The duality in the localization properties between the sparse and extremely dense RRG has been found and understood. The localization properties of the partially disordered RRG supplemented by the non-reciprocity parameter as well as the chemical potential for the 3-cycles have been analyzed numerically.

---

## Contents

<b>1</b>	<b>Introduction</b>	<b>2</b>
<b>2</b>	<b>Robustness of delocalization in partially disordered RRG</b>	<b>3</b>
2.1	The model	3
2.2	Robustness of delocalization and fractal dimension $D_2$	3
<b>3</b>	<b>Derivation of critical curve at <math>(d, \beta)</math> plane</b>	<b>5</b>
<b>4</b>	<b>Duality in localization properties between sparse and dense RRG</b>	<b>8</b>
<b>5</b>	<b>Further generalizations of the model</b>	<b>9</b>
5.1	Directed partially disordered RRG	9
5.2	Effect of chemical potential for 3-cycles	10
<b>6</b>	<b>Conclusion</b>	<b>12</b>

References	12
A Multifractal spectrum $f(\alpha)$ and fractal dimensions $D_q$	17
B Partial disorder on directed graphs	22

---

## 1 Introduction

Anderson model on the Cayley tree allows the analytic derivation of the critical disorder for the localization-delocalization phase transition [1]. More recently, the phase transition on the Anderson model with diagonal disorder on the hierarchical graphs has found its reincarnation as a toy model for the transition to many-body localized (MBL) phase in some interacting many-body systems [2]. The simplest ensemble which can be considered as the zeroth approximation to the Hilbert space of the many-body system is the random regular graph (RRG) ensemble [3–32] (see [33] for review).

It was found in [34] that the phase diagram of the Anderson model on RRG, with a finite fraction  $\beta < 1$  of disordered nodes, is different from the standard case of  $\beta = 1$  and in some region of  $(d, \beta)$ -parameter plane there are delocalized states in the central part of the spectrum, separated from the localized states by a mobility edge at arbitrarily large disorder of  $\beta$  fraction of nodes, with the box distribution. This phenomenon takes place if we have some fraction of the clean nodes. Effectively from the Hilbert-space perspective there are interacting clean and dirty subsystems in the model.

The physical motivation behind this model is given by the attempt to take into account the topologically protected zero modes in the spectrum of an interacting many-body system on the example of the Hilbert-space-graph framework. There are the overlaps of these modes with the unprotected modes hence there are links between the clean and dirty nodes in the partially disordered RRG, but this overlap does not destroy their topological nature hence the corresponding nodes in the RRG are clean.

In this study, we extend the analysis of [34] and investigate the phase structure of the partially disordered RRG in  $(\beta, d)$ -parameter space. The region in the  $(\beta, d)$  plane where the mobility edge survives at arbitrarily large disorder amplitude will be identified numerically and derived analytically for sparse and extremely dense regimes. The dependence on the graph size  $N$  of the fractal dimensions  $D_q$  and the singular spectrum  $f(\alpha)$  for eigenfunctions in the delocalized part of the spectrum is analyzed numerically. We shall explain the microscopic origin of the delocalized eigenstates and identify which aspects of the partially disordered ("two-color") graph architecture, involving the clean and dirty nodes, is crucial for the delocalization. The duality property between the mobility edges for the partially disordered RRG with degrees  $d$  and  $(N - d)$  will be shown. We shall also investigate the two generalizations of the partially disordered RRG. First, we consider the effect of the chemical potential of the short cycles on the localization pattern, suggested in [22, 35], and, second, we investigate the non-Hermitian generalization of RRG by adding the non-reciprocity to the partially disordered RRG as in [36].

Unlike several recent works [37–41], here for the emergence of the mobility edge, robust at the large potential, we need neither special flat-band structure of the disorder-free model [37–39, 42] nor correlated disorder [40, 41, 43–47]. Our model is based on the i.i.d. disorder potential on the RRG.

The rest of the article is organized as follows. In Section 2 we define the model and

present the numerical evidence for the mobility edge at arbitrarily large disorder. In Section 3 we analytically derive the critical curve in  $(\beta, d)$ -parameter space for the mobility edge. In Section 4 we find numerically and explain analytically the duality between the localization patterns for node degrees  $d$  and  $(N - d)$ . In Section 5 we present two generalizations of the model: the directed version, Sec. 5.1 and the one with the additional chemical potential for 3-cycles, Sec. 5.2. Section 6 concludes the results.

## 2 Robustness of delocalization in partially disordered RRG

In this Section we consider the numerical simulation of the RRG, with the fraction  $\beta$  of sites subject to the disorder of i.i.d. random variables  $\epsilon_i$  of the amplitude  $W/2$  taken from the uniform distribution,  $|\epsilon_i| < W/2$ . First, in Sec. 2.1 we introduce the model and, second, in Sec. 2.2 we present the numerical simulations for the spectral and localization properties of the model across the spectrum.

### 2.1 The model

In the conventional framework, one studies Anderson transition for non-interacting spinless fermions hopping over RRG with the connectivity  $d = 3$  in a diagonal disorder described by Hamiltonian

$$H = \sum_{i,j} A_{ij} \left( c_i^\dagger c_j + c_i c_j^\dagger \right) + \sum_{i=1}^{\beta N} \epsilon_i c_i^\dagger c_i . \quad (1)$$

The first sum, representing the hopping between nearest-neighbor RRG nodes  $i$  and  $j$ , is written in term of the adjacency matrix ( $A_{ij} = 1$  for nearest neighbors and  $A_{ij} = 0$  otherwise) for the regular graph,  $\sum_i A_{ij} = \sum_j A_{ij} = d$ . The second sum, running over all  $N$  nodes, represents the potential disorder. The standard fully disordered RRG ensemble, corresponding to  $\beta = 1$ , undergoes the Anderson localization transition at  $W_c = 18.16$  for  $d = 3$  [8, 11, 15, 33]. For larger  $d$  the critical disorder is usually estimated as

$$W_c(d) \simeq d \ln d . \quad (2)$$

### 2.2 Robustness of delocalization and fractal dimension $D_2$

Let us investigate numerically the properties of the states in the delocalized spectral part, found in [34] in the large  $W$  limit. As the probes we choose the density of delocalized states,  $\rho(E) = \langle \sum_{n \in \text{delocalized}} \delta(E - E_n) \rangle$ , the spectral level-spacing statistics,  $P(s)$ , with  $s_n = E_{n+1} - E_n$ , and the dependence of the fractal dimension  $D_2 \equiv -\ln(\sum_i |\psi_E(i)|^4) / \ln N$  of an eigenstate  $\psi_E(i)$  on the point in the  $(d, \beta)$  parameter plane.

First, let us demonstrate that the delocalized states survive at the very large disorder and are clearly seen numerically. Figure 1 clearly demonstrates that at large  $W$  the width of the delocalized energy range is  $W$ -independent.

Note that here and further we focus mostly on the localization,  $D_2 = 0$ , and delocalization,  $D_2 > 0$ , but not on the ergodicity,  $D_2 = 1$  versus non-ergodicity,  $0 < D_2 < 1$ . Already at  $\beta = 1$  the question of the existence of a non-ergodic phase in RRG has been a discussing point for years [4–20, 27–32] and even now the maximal system sizes of few millions,  $N \sim 10^6$  do not resolve this issue [14, 31, 32]. Therefore in this work we calculate the fractal dimensions  $D_2$  (and their generalization  $D_q$  together with the singularity spectrum  $f(\alpha)$  with the definitions given below) in the Appendix A only of finite sizes up to  $N \sim 30000$  and do not claim ergodicity or non-ergodicity.

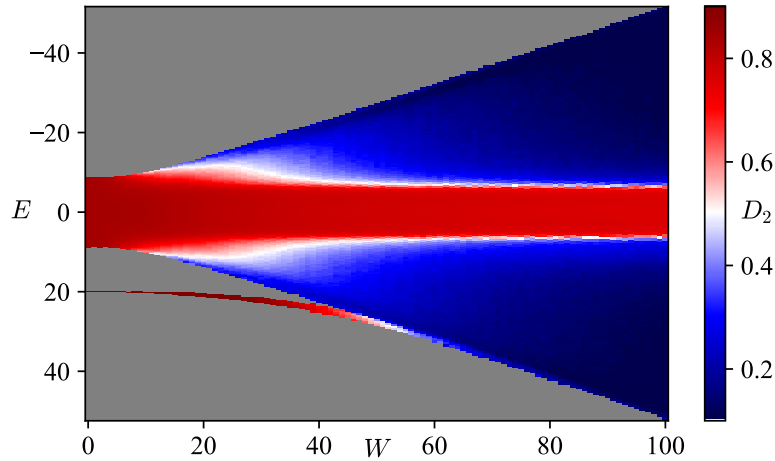


Figure 1: **Mobility edge structure versus disorder  $W$** . Color plot shows the fractal dimension  $D_2$  versus the disorder  $W$  and eigenvalues  $E$  in the partially disordered RRG of size  $N = 1024$ , with connectivity  $d = 20$ , and the fraction of disordered nodes  $\beta = 0.5$ . The data is averaged over 100 realizations.

The delocalization can be also checked via the level spacing distribution  $P(s)$ , see Fig. 2. Level spacing determines the statistics of spacing between two adjacent energy levels  $s_i = E_{i+1}^u - E_i^u$ , where  $E_i^u$  are energy levels after the unfolding procedure (see, e.g., [26] for details). There the eigenenergy statistics shows the standard repulsion inside the delocalized region and the Poisson statistics beyond the mobility edge [48].

The density of delocalized states,  $\rho(E)$  at small  $\beta$  is close to the Kesten-McKay distribution [49, 50]

$$\rho(E) = \rho_{KM}(E) = \frac{d\sqrt{4(d-1) - E^2}}{2\pi(d^2 - E^2)} \quad (3)$$

while at large  $\beta$  it becomes close to the Wigner-Dyson distribution Fig. 3. We confirm this behavior later in Eq. (17) by the analytical consideration.

It is expected since at small  $\beta$  the clean nodes form almost RRG while at larger  $\beta$  the clean-node graph get randomized by the dirty nodes. The width of the delocalized energy range has nontrivial  $(d, \beta)$  dependence, see Fig. 4(a).

There is the critical curve  $\beta_c(d)$  in the parameter space which separates the regime with and without the mobility edge, see Fig. 4(c). This is related to the percolation via the clean nodes on the partially disordered RRG, see the analytical consideration in the next section.

We have also investigated the  $N$ -dependence of the fractal dimension

$$D_q \equiv \frac{\ln(\sum_i |\psi_E(i)|^{2q})}{(1-q)\ln N} \quad (4)$$

and spectrum of fractal dimensions

$$f(\alpha) \equiv 1 + \frac{\ln P\left(\alpha = -\frac{\ln|\psi_E(i)|^2}{\ln N}\right)}{\ln N}. \quad (5)$$

The corresponding plots for  $\beta = 0.5$  and  $\beta = 0.75$  are presented in Fig. 9 – 12 in Appendix.

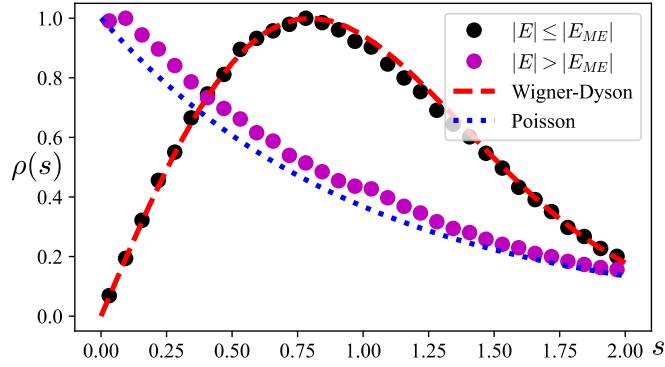


Figure 2: **Level spacing distribution between (black dots) and beyond (purple dots) the mobility edges in the partially disordered RRG of the size  $N = 1024$ , with the connectivity  $d = 20$  and the fraction of disordered nodes  $\beta = 0.5$  at the disorder  $W = 1000$ . The data is averaged over 512 realizations. Red dashed (blue dotted) line shows the Wigner-Dyson (Poisson) distribution.**

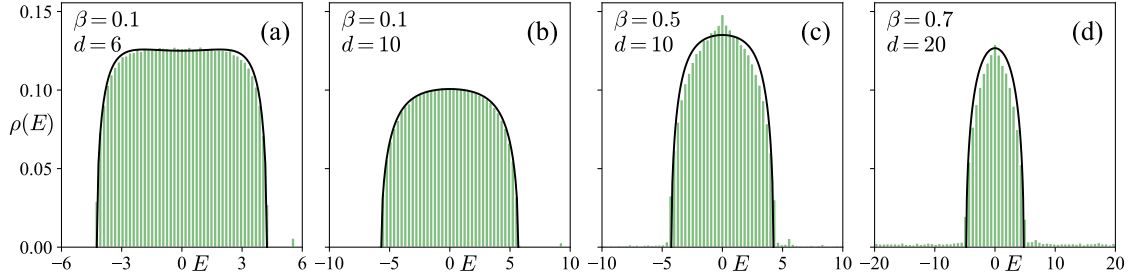


Figure 3: **Density of states of partially disordered RRG for different vertex degrees  $d$  and fractions of disordered nodes  $\beta$ .** Green-colored histograms show numerically calculated spectral densities for the size  $N = 1024$  and disorder amplitude  $W = 1000$ . The data is averaged over 100 realizations. Black lines are spectral densities, calculated from (17) for each panel. (a)  $\beta = 0.1$ ,  $d = 6$ , (b)  $\beta = 0.1$ ,  $d = 10$ , (c)  $\beta = 0.5$ ,  $d = 10$ , (d)  $\beta = 0.7$ ,  $d = 20$ .

### 3 Derivation of critical curve at $(d, \beta)$ plane

In this section, we explain why the density of the delocalized states at not very large  $\beta$  is well-approximated by the Kesten-McKay distribution with the rescaled RRG  $d^*$  and tree  $d_t^*$  degrees. This rescaling reproduces correctly the numerical result for the spectral width of the delocalized range and the critical curve at  $(d, \beta)$  plane at relatively small  $d \ll N/2$ . Note that the one-loop correction for Kesten-McKay law has been found in [51] and more general cavity analytic approach for the dense graphs has been developed in [52].

This result can be derived as follows. As on the usual RRG, let's consider cavity equations for the single-site Green's functions on clean  $G_n^*$  and dirty  $G_n'$  nodes and their

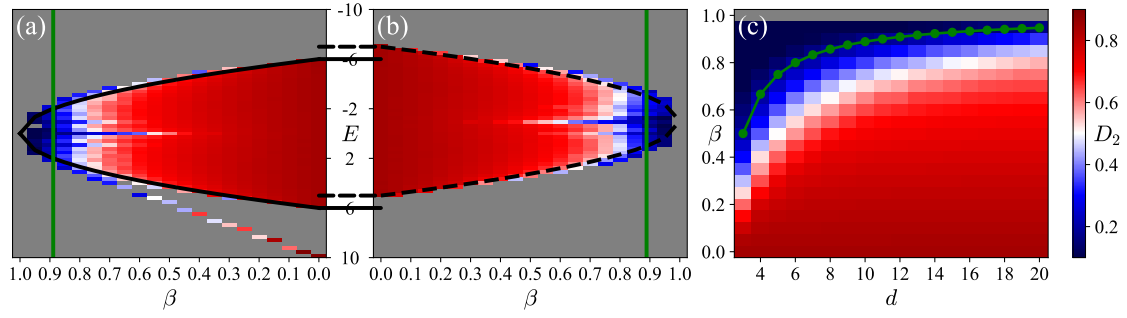


Figure 4: **Mobility edge structure versus the fraction of disordered nodes  $\beta$  and the connectivity  $d$ .** Color plots in panels (a) and (b) show the fractal dimension  $D_2$  versus  $\beta$  and eigenvalues  $E$  in the partially disordered RRG of size  $N = 1024$  at the disorder amplitude  $W = 1000$  for (a) the dilute graph with connectivity  $d = 10$  and (b) the extremely dense graph with the connectivity  $d_c = N - d \simeq N$ , which is complement to the one in (a). Black solid (dashed) line denotes mobility edge,  $|E_{me}|^2 = 4(1 - \beta)(d - 1)$ , Eq. (18), ( $|E_{me} + 1|^2 = 4(1 - \beta)(d - 1)$ ). (c) Color plot of the average fractal dimensions  $D_2$  in the central band  $|E| < E_{ME}$  in the partially disordered RRG versus  $\beta$  and  $d$  at  $W = 1000$ . Green solid lines in all panels show the critical curve  $\beta_c$ , given by (18). All the data is averaged over 25 realizations.

tree counterparts  $G_{n \rightarrow a}^*$  and  $G_{n \rightarrow a}'$  with the removed link from  $n$  to its ancestor  $a$ .

$$\begin{cases} \frac{1}{G_n^*} = E + i\eta - \sum_{m=1}^{k_n} G_{i_m^* \rightarrow n}^* - \sum_{m=1}^{d-k_n} G_{i'_m \rightarrow n}' \\ \frac{1}{G_n'} = E + i\eta - \varepsilon_i - \sum_{m=1}^{k_n} G_{i_m^* \rightarrow n}^* - \sum_{m=1}^{d-k_n} G_{i'_m \rightarrow n}' \\ \frac{1}{G_{n \rightarrow a}^*} = E + i\eta - \sum_{m=1}^{l_n} G_{i_m^* \rightarrow n}^* - \sum_{m=1}^{d-1-l_n} G_{i'_m \rightarrow n}' \\ \frac{1}{G_{n \rightarrow a}'} = E + i\eta - \varepsilon_i - \sum_{m=1}^{l_n} G_{i_m^* \rightarrow n}^* - \sum_{m=1}^{d-1-k_n} G_{i'_m \rightarrow n}' \end{cases}, \quad (6)$$

where  $i_m^*$  and  $i'_m$  are the indices, enumerating the pure and disordered sites on the tree, the ancestor of which is  $n$ ,  $k_n$  and  $l_n$  are numbers of clean descendants of  $n$  on the RRG ( $G_n$ ) and on the tree ( $G_{n \rightarrow a}$ ), respectively. It is important to note that the total number of the descendants of  $n$  for the tree is given by a branching number  $d_t = d - 1$ , while for the RRG, where each point is locally a root of the tree, it is given by the vertex degree  $d$ .

The number of clean nearest descendants of any node  $n$  obeys binomial distribution

$$p_{\tilde{d}}(k) = \binom{\tilde{d}}{k} (1 - \beta)^k \beta^{\tilde{d}-k}, \quad (7)$$

with  $\tilde{d} = d_t$ ,  $k = l_n$  for the tree ( $p_{d_t}(l_n)$ ) and  $\tilde{d} = d$ ,  $k = k_n$  for the RRG ( $p_d(k_n)$ ). In both cases, for large  $(1 - \beta)\tilde{d} \gg 1$  this distribution is well approximated by the normal distribution with the mean and the variance given by

$$\langle k \rangle_{\tilde{d}} = \sum_k p_{\tilde{d}}(k) k = (1 - \beta)\tilde{d} \quad (8)$$

$$\sigma_{\tilde{d}}^2 = \sum_k p_{\tilde{d}}(k) (k - \langle k \rangle_{\tilde{d}})^2 = \beta(1 - \beta)\tilde{d} \quad (9)$$

Let's consider the simplest approximation at large  $W$  by keeping in the equation for the dirty nodes only the disorder term which yields

$$G'_n \propto W^{-1} \quad (10)$$

and substitute this solution into the equation for the clean nodes. In the limit  $W \rightarrow \infty$  the effects of dirty nodes are subleading hence we get the equation for clean nodes

$$\frac{1}{G_n^*} = E + i\eta - \sum_{m=1}^{k_n} G_{i_m^* \rightarrow n}^* \quad (11)$$

$$\frac{1}{G_{n \rightarrow a}^*} = E + i\eta - \sum_{m=1}^{l_n} G_{i_m^* \rightarrow n}^* . \quad (12)$$

These equations evidently yield the RRG KM spectral density, but now both with fluctuating and rescaled  $d^* = k_n$  and  $d_t^* = l_n$ . For large enough  $\langle k \rangle_{d_t} \gg 1$  the corresponding rescaled parameters in the most realizations are given by their mean values

$$d^* = \langle k \rangle_d = (1 - \beta)d, \quad d_t^* = \langle l \rangle_{d_t} = (1 - \beta)d_t \quad (13)$$

and their relative fluctuations are small as  $\sigma_d/d^* \sim \sqrt{\beta/d^*} \ll \beta^{1/2} \leq 1$ . The critical value  $\beta_c$ , when the clean nodes do not form a connected tree-like graph, can be derived from the equation  $d_t^*(\beta_c) = 1$ .

Note that, unlike the regular case, both rescaled parameters  $d^*$  and  $d_t^*$  are *not* anymore related to each other via  $d^* = d_t^* + 1$  (similarly to [53]).

The generalized KM distribution can be obtained from Eqs. (11) and (12). Assuming that  $G_{n \rightarrow a}^*$  is self-averaging, one can rewrite the latter of two equations as a self-consistent equation on the mean  $\langle G_{n \rightarrow a}^* \rangle = G_{\rightarrow}^*$  as follows

$$\frac{1}{G_{\rightarrow}^*} = E + i\eta - d_t^* G_{\rightarrow}^* , \quad (14)$$

which immediately gives the solution

$$G_{\rightarrow}^* = \frac{E + i\sqrt{4d_t^* - E^2}}{2d_t^*}, \quad d_t^* = (1 - \beta)(d - 1). \quad (15)$$

with the semi-circular density of states  $\rho_{\rightarrow} = \text{Im } G_{\rightarrow}^* / \pi$ .

The generalized KM distribution is given by the equation (11) for  $\langle G_n^* \rangle = G^*$  with  $k_n \simeq d^* = (1 - \beta)d$

$$G^* = \frac{1}{E + i\eta - d^* G_{\rightarrow}^*} = \frac{(d - 2)E + id\sqrt{4d_t^* - E^2}}{2[d^2(1 - \beta) - E^2]} . \quad (16)$$

This gives for the density of states  $\rho$

$$\rho(E) = \frac{\text{Im } G^*}{\pi} = \frac{d\sqrt{4(d - 1)(1 - \beta) - E^2}}{2\pi[d^2(1 - \beta) - E^2]} . \quad (17)$$

Like in the standard KM distribution, the critical value  $\beta_c$  is defined as percolation threshold  $d_t^* = 1$  on the tree with the branching number  $d_t^*$

$$1 - \beta_c = \frac{1}{d - 1} \rightarrow \beta_c = 1 - \frac{1}{d - 1}. \quad (18)$$

If  $\beta \leq \beta_c$ , the graph of clean nodes has a giant connected component, and the wave functions on this component are delocalized. If  $\beta > \beta_c$ , the graph of clean nodes separates into disconnected components, average size  $n$  of each of those is small compared to the network size,  $n \ll N$ . Localized eigenstates in Fig. 4(a) significantly below threshold appear due to the isolated pure nodes at  $\lambda = 0$  and connected pairs of pure nodes at  $\lambda = \pm 1$ .

## 4 Duality in localization properties between sparse and dense RRG

The numerical simulation in Fig. 4(a), (b) shows that for the dense RRG at large  $d$ , when  $|N - d| \ll N$ , the energy interval, where the states are delocalized, and the mobility edge curve in the  $(d, \beta)$ -plane exists as well. The width of this interval  $\Delta E$  is

$$\Delta E = (1 - \beta) \min [d, (N - d - 1)] - 1$$

that corresponds to the results of the complementary graph with  $d_c = N - d - 1 \ll N$ .

For the adjacency matrix, consisting of 0 and 1, and for the symmetric disorder distribution, the above mapping to the complimentary graph can be straightforwardly understood via the rank-1 perturbation of the initial problem, see [54].

Indeed, using the eigenvalues  $E_n^0$  and eigenvectors  $|E_n^0\rangle$  of a certain realization of the problem on the initial (complimentary) graph with the connectivity  $d_c \ll N$  and the diagonal disorder  $\varepsilon_i$ , one can straightforwardly write the Hamiltonian of the dense model (with  $d = N - d_c \simeq N$ ) as follows

$$H = - \sum_n E_n^0 |E_n^0\rangle \langle E_n^0| + |1\rangle \langle 1| - I . \quad (19)$$

Here  $\langle i|1\rangle = 1$  for all sites  $i$  and  $I$  is the identity matrix, as the vector  $|1\rangle$  of ones is not normalized. Note that for any disorder realization on the initial (complimentary) graph  $\epsilon_{i,c}$ , the effective disorder realization in the dense one changes its sign  $\epsilon_i = -\epsilon_{i,c}$ .

The peculiar property of the complimentary model is that the part  $|1\rangle \langle 1|$ , non-diagonal in the eigenstate basis of the initial problem  $\{|E_n^0\rangle\}$ , is a rank-1 matrix and therefore this dense model can be solved using the simplest Bethe ansatz solution of the Richardson's model [55–59].

$$\sum_n \frac{|\langle E_n^0|1\rangle|^2}{E + E_n^0 + 1} = 1, \quad (20)$$

$$|E\rangle = C_E \sum_n \frac{\langle E_n^0|1\rangle}{E + E_n^0 + 1} |E_n^0\rangle, \quad (21)$$

$$C_E^{-2} = \sum_n \frac{|\langle E_n^0|1\rangle|^2}{(E + E_n^0 + 1)^2}. \quad (22)$$

From the literature [58, 60–63] it is known that, as soon as  $|\langle E_n^0|1\rangle|^2$  is more or less homogeneous versus  $n$  and  $W \ll N$ , all but one new eigenvalues, being the solutions of Eq. (20),  $E = E_n$  (shifted by 1 in our case due to the presence of  $I$  in the equation) are located in between the old ones  $-E_{N-n+1}^0 < E_n + 1 < -E_{N-n}^0$  and the eigenstates are power-law localized in the eigenbasis of the initial problem with the power-law exponent 2,  $|\langle E_{N-n}^0|E_m\rangle|^2 \sim 1/|m - n|^2$ . This property is related to the fact that for  $W \ll d \sim N$  all but one eigenstates are nearly orthogonal to  $|1\rangle$ .

The only high-energy level (not shown in Fig. 4(b)), which is not orthogonal to  $|1\rangle$  takes the large energy of the order of  $E_N \sim N$ . As soon as the diagonal disorder  $W \ll N$ , this vector is delocalized as  $|E_N\rangle \simeq |1\rangle / \sqrt{N}$ .

This immediately means that

- The width and the profile of the band are the same in the initial and complementary problems;



- The localization and fractal properties  $D_q$  are also the same, at least for  $q > 1/2$ , where the power-law localization tails are not important;
- The only difference appears at  $W \ll N$ , when there is the high-energy level at  $E_N \simeq N$ , while the bulk bandwidth is shifted by  $-1$  (due to the same trace of both initial and complimentary matrices).

All these properties have been numerically investigated in Fig. 4(b), please compare with the panel (a) to see the shift of energy by 1.

## 5 Further generalizations of the model

Next, we consider several generalizations of the partially disordered RRG model to the non-reciprocal version of it [36], see Sec. 5.1, and to the RRG, perturbed by a chemical potential of short 3-cycles [22, 35], see Sec. 5.2, and investigate numerically the localization and multifractal properties of these models.

### 5.1 Directed partially disordered RRG

In this section, we consider the localization in the Anderson model on a partially directed RRG with the non-Hermitian spectrum in the partially disordered case, dubbed as  $\beta$ -deformation of RRG. The two-parametric non-Hermitian model in the full generality will be presented in [36].

The model in [36] uses two parameters that correspond to the reciprocity and the hopping asymmetry. In this work, only dependence on reciprocity  $0 \leq r \leq 1$  is studied. A traditional way to define network reciprocity involves the ratio of the number of bidirectional connections to the number of all, bidirectional and unidirectional, connections. We modify the RRG network as follows: with the probability  $r$ , we replace an undirected edge by two oppositely directed ones, with weights of 1 each. Otherwise, with probability  $1 - r$ , the undirected edge is changed to one directed in a random direction, with the weight of 2. Therefore, the total bandwidth of the link between connected nodes is constant and equal to 2. If  $r = 0$  the graph becomes an oriented directed RRG graph, while at  $r = 1$  the graph is equivalent to the standard undirected RRG. At certain ranges of parameters, this model has a tendency to become undiagonalizable due to the existence of exceptional points, see [36] for more details. To overcome the problem, small perturbation feedback  $\epsilon = 2 \times 10^{-5}$  is added to unidirected edges.

The representative realizations of complex-valued spectra for RRG with the connectivity  $d = 8$  for different  $r$ ,  $W$  and for  $\beta = 0.5$  and  $\beta = 1.0$  are shown in Fig. 5. All the points in these plots are colored by the value of the fractal dimension  $D_2$  of a product of left and right eigenvectors in a biorthogonal basis,  $\langle \psi_i^L | \psi_j^R \rangle = \delta_{ij}$ . For more details, please see Fig. 13, 14 in Appendix B.

Let us summarize the effects of competition of  $\beta$  and  $r$  parameters at large  $W$

- Instead of the mobility edge of the undirected case,  $r = 1$ , for  $r < 1$ ,  $\beta < 1$  we have the mobility curve in the complex plane. At  $\beta = 0.5$  and large  $W$  the spread of the imaginary parts of the delocalized states is independent of  $W$ . The imaginary part of the localized states at large  $W$  vanishes. The latter is natural as the diagonal disorder, which is dominant, is real, see [64].
- With the parameter  $r$ , the width of the delocalized region along the real axis varies in the same order as the initial model.

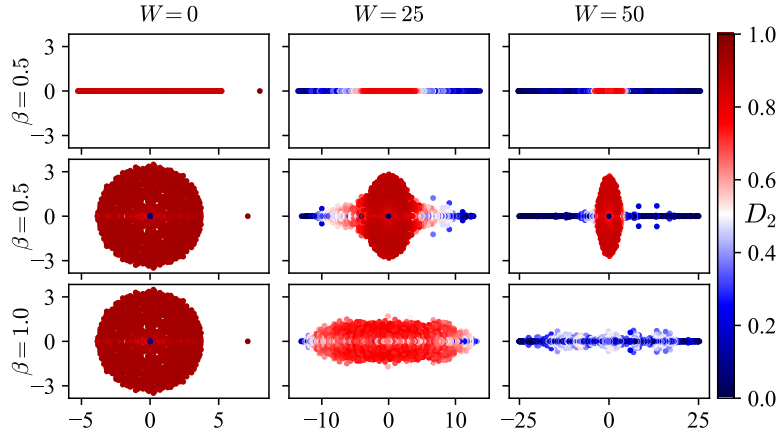


Figure 5: **Representative realizations of the complex-valued spectra in partially disordered and partially directed RRG** of the size  $N = 1024$ , with the connectivity  $d = 8$  for different disorder strengths  $W$  and the fraction  $\beta$  of disordered nodes. Color coding corresponds to the fractal dimension  $D_2$  of a product of left and right eigenvectors in a biorthogonal basis,  $\langle \psi_i^L | \psi_j^R \rangle = \delta_{ij}$ , for each point in the parameter space. The top row corresponds to an undirected Hermitian graph,  $r = 1$ , while the second and third ones – to the directed graphs, with the reciprocity parameter  $r = 0.125$  determined as the fraction of bidirected connections to all connections.

- At  $r < 1$ ,  $\beta < 1$  the non-reciprocity leads to the emergence of the island of the localized states inside the delocalized region. Similarly to [36], this island is related to the emergence of the topologically equivalent nodes (TEN) as well as the nodes with only incoming edges (node inflows). This localized island disappears at large enough  $r$ .

## 5.2 Effect of chemical potential for 3-cycles

For completeness, let us consider the effect of the  $\mu_3$ -deformation of the RRG by a chemical potential of the 3-cycles on the localization of the partially disordered RRG. For the  $\beta = 1$ , some observations concerning the localization in  $\mu_3$ -deformed theory can be found in [22] and the thorough analysis which uncovered quite rich phase structure has been performed in [35] for various systems sizes  $N$ , node degrees  $d$ , and the cycle lengths  $k$ , corresponding to  $\mu_k$ . In particular, there are four different phases at the  $(\mu_3, d)$  parameter space: unclustered,  $\mu_3 < \mu_{3,TEN}$ , TEN-scarred,  $\mu_{3,TEN} < \mu_3 < \mu_c$ , and two clustered ones,  $\mu_3 > \mu_c, \mu_{3,TEN}$ : ideal and interacting ones. At leading terms in  $N$  of the above critical line are given by  $\mu_{3,TEN} \sim \frac{(d-2) \ln N}{(d-1)}$  and  $\mu_c \sim \frac{3(d-2) \ln N}{d(d-1)}$ , please see [35] for more details.

Here we shall consider numerically some effects of the  $\beta$ -deformation in the  $\mu_3$ -deformed RRG. In Figure 6 we present the localization pattern for fractal dimension at  $\beta = 0.5$  in the  $(W, E)$ -plane, while in Fig. 7 we show its behavior in the  $(\mu_3, E)$ -plane.

Figure 7 shows the effect of  $\mu_3$  on the partially disordered RRG. At small  $\mu_3 < \mu_c$  in the unclustered phase, both the dependence of  $D_2$  on the parameters and the position remains the same as in Figure 1. At  $\mu_3 > \mu_c$  (see Fig. 7 at  $\mu_3 > 1.25$ ), the system undergoes the clusterization transition [35]. The dependence of  $D_2$  on  $W$  changes, as shown in Figure 6. The localization in the  $\beta$ -deformed RRG model occurs in each cluster separately. This

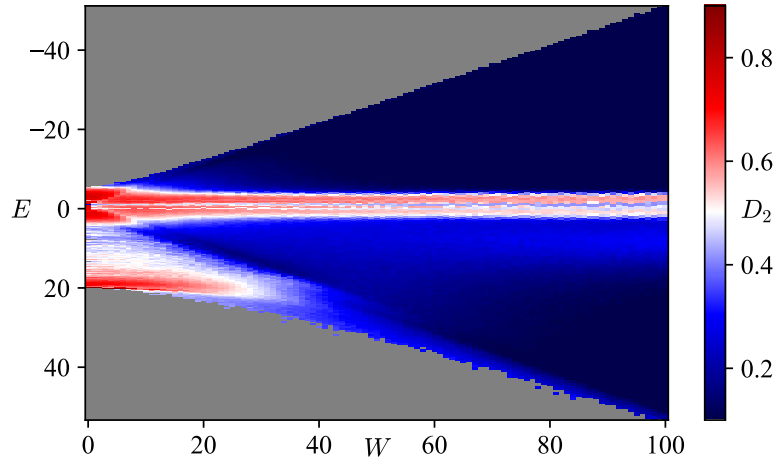


Figure 6: Color plot of the fractal dimension  $D_2$  versus  $W$  and  $E$  in the partially disordered RRG of the size  $N = 1024$ , modified by the short 3-cycles, with  $\beta = 0.5$  and  $\mu_3 = 2$  in the clustered phase. Each point of a color plot is averaged over 20 structural and 5 disorder realizations.

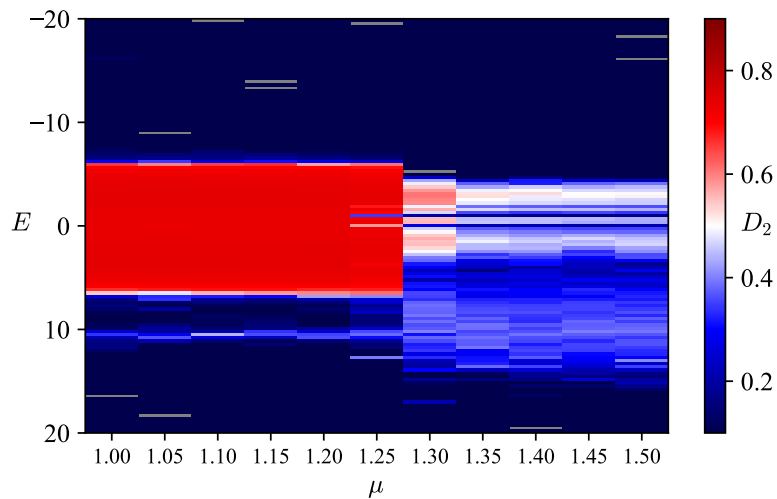


Figure 7: Color plot of the fractal dimension  $D_2$  versus  $\mu_3$  and  $E$  in the partially disordered RRG of the size  $N = 1024$ , modified by the short 3-cycles, with  $\beta = 0.5$ ,  $W = 1000$ . Each point of a color plot is averaged over 5 structural and 5 disorder realizations.

effectively replaces  $N$  by  $d + 1$  and suppresses  $D_q$  value in Fig 7. In clustered phase, the center of the continuous spectrum part shifts to  $-1$  because the graph consists of dense clusters of triangles and narrows due to the change of spectral density from KM distribution to triangular shape distribution, like in the diagonal disorder-free case.

## 6 Conclusion

In this study we have clarified the mechanism behind the robustness of the delocalized energy range at arbitrarily large disorder, found in [34]. The system involves interacting clean and dirty subsystems and the delocalized region at the  $(d, \beta)$ -parameter plane corresponds to an effective problem solely on the clean nodes, with the renormalized RRG and tree degrees, at the large disorder. This result has been obtained analytically in the leading approximation in  $1/W$  and confirmed numerically for sparse and dense regimes. The effects of non-Hermitian perturbation of  $\beta$ -deformed RRG and chemical potential for the 3-cycles have been as well investigated.

The pattern of the appearance of the controllable mobility edge we have found provides the additional insights for the account of the topologically protected modes of the interacting many-body systems in the Hilbert space framework. In this respect it would be of a particular interest to generalize the effect of  $\beta$ -deformation to the many-body Hilbert space structures, like a hypercube graph in the quantum random energy model [65, 66]. It is also interesting to consider a randomly distributed  $\beta$  parameter and the effects of the non-Hermitian diagonal disorder, which may lead to the localization enhancement [67–70], unlike the usual non-reciprocity [64]. If the RRG ensemble is considered as the discrete model for the 2d quantum gravity the Anderson model corresponds to the massive field coupled to the fluctuating geometry. The case of the Anderson model on partially disordered RRG corresponds to the situation when there are zero modes of the field localized at some defects. It would be interesting to develop this framework further.

## Acknowledgements

We thank A. Scardicchio for fruitful discussions. A.G. thanks Nordita and IHES where the parts of this work have been done for the hospitality and support.

**Funding information** I. M. K. acknowledges the support by the Russian Science Foundation, Grant No. 21-12-00409.

## References

- [1] R. Abou-Chacra, D. Thouless and P. Anderson, *A selfconsistent theory of localization*, Journal of Physics C: Solid State Physics **6**(10), 1734 (1973), doi:10.1088/0022-3719/6/10/009.
- [2] B. L. Altshuler, Y. Gefen, A. Kamenev and L. S. Levitov, *Quasiparticle lifetime in a finite system: A nonperturbative approach*, Phys. Rev. Lett. **78**, 2803 (1997), doi:10.1103/PhysRevLett.78.2803.

- [3] A. D. Mirlin and Y. V. Fyodorov, *Localization transition in the anderson model on the bethe lattice: Spontaneous symmetry breaking and correlation functions*, Nuclear Physics B **366**(3), 507 (1991), doi:[https://doi.org/10.1016/0550-3213\(91\)90028-V](https://doi.org/10.1016/0550-3213(91)90028-V).
- [4] G. Biroli, A. C. Ribeiro-Teixeira and M. Tarzia, *Difference between level statistics, ergodicity and localization transitions on the Bethe lattice*, URL <https://arxiv.org/abs/1211.7334> (2012), 1211.7334.
- [5] G. Biroli and M. Tarzia, *Delocalized glassy dynamics and many-body localization*, Phys. Rev. B **96**, 201114(R) (2017), doi:10.1103/PhysRevB.96.201114.
- [6] G. Biroli and M. Tarzia, *Delocalization and ergodicity of the Anderson model on Bethe lattices*, URL <http://arxiv.org/abs/1810.07545> (2018), 1810.07545.
- [7] G. Biroli and M. Tarzia, *Anomalous dynamics on the ergodic side of the many-body localization transition and the glassy phase of directed polymers in random media*, Phys. Rev. B **102**, 064211 (2020), doi:10.1103/PhysRevB.102.064211.
- [8] A. De Luca, B. Altshuler, V. Kravtsov and A. Scardicchio, *Anderson localization on the Bethe lattice: Nonergodicity of extended states*, Phys. Rev. Lett. **113**(4), 046806 (2014), doi:10.1103/PhysRevLett.113.046806.
- [9] B. L. Altshuler, E. Cuevas, L. B. Ioffe and V. E. Kravtsov, *Nonergodic phases in strongly disordered random regular graphs*, Phys. Rev. Lett. **117**, 156601 (2016), doi:10.1103/PhysRevLett.117.156601.
- [10] B. L. Altshuler, L. B. Ioffe and V. E. Kravtsov, *Multifractal states in self-consistent theory of localization: analytical solution*, URL <http://arxiv.org/abs/1610.00758> (2016), 1610.00758.
- [11] V. E. Kravtsov, B. L. Altshuler and L. B. Ioffe, *Non-ergodic delocalized phase in Anderson model on Bethe lattice and regular graph*, Annals of Physics **389**, 148 (2018), doi:<https://doi.org/10.1016/j.aop.2017.12.009>.
- [12] I. García-Mata, O. Giraud, B. Georgeot, J. Martin, R. Dubertrand and G. Lemarié, *Scaling theory of the Anderson transition in random graphs: Ergodicity and universality*, Phys. Rev. Lett. **118**, 166801 (2017), doi:10.1103/PhysRevLett.118.166801.
- [13] I. García-Mata, J. Martin, R. Dubertrand, O. Giraud, B. Georgeot and G. Lemarié, *Two critical localization lengths in the Anderson transition on random graphs*, Phys. Rev. Research **2**, 012020 (2020), doi:10.1103/PhysRevResearch.2.012020.
- [14] I. García-Mata, J. Martin, O. Giraud, B. Georgeot, R. Dubertrand and G. Lemarié, *Critical properties of the Anderson transition on random graphs: Two-parameter scaling theory, kosterlitz-thouless type flow, and many-body localization*, Phys. Rev. B **106**, 214202 (2022), doi:10.1103/PhysRevB.106.214202.
- [15] G. Parisi, S. Pascazio, F. Pietracaprina, V. Ros and A. Scardicchio, *Anderson transition on the Bethe lattice: an approach with real energies*, Journal of Physics A: Mathematical and Theoretical **53**(1), 014003 (2019), doi:10.1088/1751-8121/ab56e8.
- [16] K. S. Tikhonov and A. D. Mirlin, *Fractality of wave functions on a Cayley tree: Difference between tree and locally treelike graph without boundary*, Phys. Rev. B **94**, 184203 (2016), doi:10.1103/PhysRevB.94.184203.

- [17] K. S. Tikhonov, A. D. Mirlin and M. A. Skvortsov, *Anderson localization and ergodicity on random regular graphs*, Phys. Rev. B **94**, 220203(R) (2016), doi:10.1103/PhysRevB.94.220203.
- [18] M. Sonner, K. S. Tikhonov and A. D. Mirlin, *Multifractality of wave functions on a Cayley tree: From root to leaves*, Phys. Rev. B **96**, 214204 (2017), doi:10.1103/PhysRevB.96.214204.
- [19] K. S. Tikhonov and A. D. Mirlin, *Statistics of eigenstates near the localization transition on random regular graphs*, Phys. Rev. B **99**, 024202 (2019), doi:10.1103/PhysRevB.99.024202.
- [20] K. S. Tikhonov and A. D. Mirlin, *Eigenstate correlations around many-body localization transition*, Phys. Rev. B **103**, 064204 (2021), doi:10.1103/PhysRevB.103.064204.
- [21] V. Avetisov, M. Hovhannisyan, A. Gorsky, S. Nechaev, M. Tamm and O. Valba, *Eigenvalue tunneling and decay of quenched random network*, Physical Review E **94**(6), 062313 (2016).
- [22] V. Avetisov, A. Gorsky, S. Nechaev and O. Valba, *Localization and non-ergodicity in clustered random networks*, Journal of Complex Networks **8**(2), cnz026 (2020).
- [23] O. Valba and A. Gorsky, *Interacting thermofield doubles and critical behavior in random regular graphs*, Physical Review D **103**(10), 106013 (2021).
- [24] S. Bera, G. De Tomasi, I. M. Khaymovich and A. Scardicchio, *Return probability for the Anderson model on the random regular graph*, Physical Review B **98**(13), 134205 (2018).
- [25] G. De Tomasi, S. Bera, A. Scardicchio and I. M. Khaymovich, *Subdiffusion in the Anderson model on the random regular graph*, Phys. Rev. B **101**, 100201(R) (2020), doi:10.1103/PhysRevB.101.100201.
- [26] L. Colmenarez, D. J. Luitz, I. M. Khaymovich and G. De Tomasi, *Subdiffusive thouless time scaling in the Anderson model on random regular graphs*, Phys. Rev. B **105**, 174207 (2022), doi:10.1103/PhysRevB.105.174207.
- [27] V. E. Kravtsov, I. M. Khaymovich, B. L. Altshuler and L. B. Ioffe, *Localization transition on the random regular graph as an unstable tricritical point in a log-normal Rosenzweig-Porter random matrix ensemble*, URL <https://arxiv.org/abs/2002.02979>, 2002.02979 (2020), 2002.02979.
- [28] I. M. Khaymovich, V. E. Kravtsov, B. L. Altshuler and L. B. Ioffe, *Fragile ergodic phases in logarithmically-normal Rosenzweig-Porter model*, Phys. Rev. Research **2**, 043346 (2020), doi:10.1103/PhysRevResearch.2.043346.
- [29] I. M. Khaymovich and V. E. Kravtsov, *Dynamical phases in a “multifractal” Rosenzweig-Porter model*, SciPost Phys. **11**, 45 (2021), doi:10.21468/SciPostPhys.11.2.045.
- [30] J.-N. Herre, J. F. Karcher, K. S. Tikhonov and A. D. Mirlin, *Ergodicity-to-localization transition on random regular graphs with large connectivity and in many-body quantum dots* (2023), doi:10.48550/arXiv.2302.06581, 2302.06581.
- [31] M. Pino, *Scaling up the anderson transition in random-regular graphs*, Phys. Rev. Res. **2**, 042031 (2020), doi:10.1103/PhysRevResearch.2.042031.

- [32] C. Vanoni, B. L. Altshuler, V. E. Kravtsov and A. Scardicchio, *Renormalization group analysis of the Anderson model on random regular graphs*, URL <http://arxiv.org/abs/2306.14965> (2023), 2306.14965.
- [33] K. S. Tikhonov and A. D. Mirlin, *From Anderson localization on random regular graphs to many-body localization*, *Annals of Physics* p. 168525 (2021), doi:10.1016/j.aop.2021.168525.
- [34] O. Valba and A. Gorsky, *Mobility edge in the Anderson model on partially disordered random regular graphs*, *JETP Letters* **116**(6), 398 (2022), doi:10.1134/S0021364022601750.
- [35] D. Kochergin, I. M. Khaymovich, O. Valba and A. Gorsky, *Anatomy of the fragmented hilbert space: Eigenvalue tunneling, quantum scars, and localization in the perturbed random regular graph*, *Phys. Rev. B* **108**, 094203 (2023), doi:10.1103/PhysRevB.108.094203.
- [36] D. Kochergin, V. Tiselko and A. Onuchin, *Localization transition in non-hermitian systems depending on reciprocity and hopping asymmetry*, In preparation.
- [37] C. Danieli, J. D. Bodyfelt and S. Flach, *Flat-band engineering of mobility edges*, *Phys. Rev. B* **91**, 235134 (2015), doi:10.1103/PhysRevB.91.235134.
- [38] A. Ahmed, A. Ramachandran, I. M. Khaymovich and A. Sharma, *Flat band based multifractality in the all-band-flat diamond chain*, *Phys. Rev. B* **106**, 205119 (2022), doi:10.1103/PhysRevB.106.205119.
- [39] S. Lee, A. Andreanov and S. Flach, *Critical-to-insulator transitions and fractality edges in perturbed flat bands*, *Phys. Rev. B* **107**, 014204 (2023), doi:10.1103/PhysRevB.107.014204.
- [40] Y. Wang, X. Xia, L. Zhang, H. Yao, S. Chen, J. You, Q. Zhou and X.-J. Liu, *One-dimensional quasiperiodic mosaic lattice with exact mobility edges*, *Phys. Rev. Lett.* **125**, 196604 (2020), doi:10.1103/PhysRevLett.125.196604.
- [41] J. Gao, I. M. Khaymovich, X.-W. Wang, Z.-S. Xu, A. Iovan, G. Krishna, A. V. Balatsky, V. Zwiller and A. W. Elshaari, *Experimental probe of multi-mobility edges in quasiperiodic mosaic lattices*, URL <https://arxiv.org/abs/2306.10829> (2023), 2306.10829.
- [42] J. D. Bodyfelt, D. Leykam, C. Danieli, X. Yu and S. Flach, *Flat-bands under correlated perturbations*, *Phys. Rev. Lett.* **113**, 236403 (2014), doi:10.1103/PhysRevLett.113.236403.
- [43] J. Biddle and S. Das Sarma, *Predicted mobility edges in one-dimensional incommensurate optical lattices: An exactly solvable model of anderson localization*, *Phys. Rev. Lett.* **104**, 070601 (2010), doi:10.1103/PhysRevLett.104.070601.
- [44] S. Ganeshan, J. H. Pixley and S. Das Sarma, *Nearest neighbor tight binding models with an exact mobility edge in one dimension*, *Phys. Rev. Lett.* **114**, 146601 (2015), doi:10.1103/PhysRevLett.114.146601.
- [45] M. Gonçalves, B. Amorim, E. V. Castro and P. Ribeiro, *Hidden dualities in 1D quasiperiodic lattice models*, *SciPost Phys.* **13**, 046 (2022), doi:10.21468/SciPostPhys.13.3.046.

- [46] T. Liu, X. Xia, S. Longhi and L. Sanchez-Palencia, *Anomalous mobility edges in one-dimensional quasiperiodic models*, SciPost Phys. **12**, 027 (2022), doi:10.21468/SciPostPhys.12.1.027.
- [47] M. Gonçalves, P. Ribeiro and I. M. Khaymovich, *Quasiperiodicity hinders ergodic floquet eigenstates*, Accepted to Phys. Rev. B (2023), 2306.12479.
- [48] M. Mehta, *Random Matrices*, ISSN. Elsevier Science, ISBN 9780080474113 (2004).
- [49] H. Kesten, *Symmetric random walks on groups*, Transactions of the American Mathematical Society **92**(2), 336 (1959), doi:10.1090/S0002-9947-1959-0109367-6.
- [50] B. D. McKay, *The expected eigenvalue distribution of a large regular graph*, Linear Algebra and its Applications **40**, 203 (1981), doi:https://doi.org/10.1016/0024-3795(81)90150-6.
- [51] F. L. Metz, G. Parisi and L. Leuzzi, *Finite-size corrections to the spectrum of regular random graphs: An analytical solution*, Physical Review E **90**(5) (2014), doi:10.1103/physreve.90.052109.
- [52] J. D. Silva and F. L. Metz, *Analytic solution of the resolvent equations for heterogeneous random graphs: spectral and localization properties*, Journal of Physics: Complexity **3**(4), 045012 (2022), doi:10.1088/2632-072X/aca9b1.
- [53] P. Sierant, M. Lewenstein and A. Scardicchio, *Universality in Anderson localization on random graphs with varying connectivity*, URL <https://scipost.org/submissions/2205.14614v3/>, Accepted to SciPost Phys. 15 (2023) (2022), 2205.14614.
- [54] E. Bogomolny, *Modification of the Porter-Thomas distribution by rank-one interaction*, Phys. Rev. Lett. **118**, 022501 (2017), doi:10.1103/PhysRevLett.118.022501.
- [55] R. Richardson, *A restricted class of exact eigenstates of the pairing-force Hamiltonian*, Phys. Lett. **3**(6), 277 (1963), doi:10.1016/0031-9163(63)90259-2.
- [56] R. Richardson and N. Sherman, *Exact eigenstates of the pairing-force Hamiltonian*, Nuclear Physics **52**, 221 (1964), doi:10.1016/0029-5582(64)90687-X.
- [57] A. Ossipov, *Anderson localization on a simplex*, J. Phys. A **46**, 105001 (2013), doi:10.1088/1751-8113/46/10/105001.
- [58] R. Modak, S. Mukerjee, E. A. Yuzbashyan and B. S. Shastry, *Integrals of motion for one-dimensional Anderson localized systems*, New J. Phys. **18**, 033010 (2016), doi:10.1088/1367-2630/18/3/033010.
- [59] M. C. Cambiaggio, A. M. F. Rivas and M. Saraceno, *Integrability of the pairing Hamiltonian*, Nuclear Physics A **624**(2), 157 (1997), doi:10.1016/S0375-9474(97)00418-1.
- [60] P. A. Nosov, I. M. Khaymovich and V. E. Kravtsov, *Correlation-induced localization*, Physical Review B **99**(10), 104203 (2019), doi:10.1103/PhysRevB.99.104203.
- [61] P. A. Nosov and I. M. Khaymovich, *Robustness of delocalization to the inclusion of soft constraints in long-range random models*, Phys. Rev. B **99**, 224208 (2019), doi:10.1103/PhysRevB.99.224208.
- [62] V. R. Motamarri, A. S. Gorsky and I. M. Khaymovich, *Localization and fractality in disordered Russian Doll model*, SciPost Phys. **13**, 117 (2022), doi:10.21468/SciPostPhys.13.5.117.



- [63] A. G. Kutlin and I. M. Khaymovich, *Emergent fractal phase in energy stratified random models*, SciPost Phys. **11**, 101 (2021), doi:10.21468/SciPostPhys.11.6.101.
- [64] N. Hatano and D. R. Nelson, *Localization transitions in non-Hermitian quantum mechanics*, Phys. Rev. Lett. **77**, 570 (1996), doi:10.1103/PhysRevLett.77.570.
- [65] C. R. Laumann, A. Pal and A. Scardicchio, *Many-body mobility edge in a mean-field quantum spin glass*, Phys. Rev. Lett. **113**, 200405 (2014), doi:10.1103/PhysRevLett.113.200405.
- [66] C. L. Baldwin, C. R. Laumann, A. Pal and A. Scardicchio, *The many-body localized phase of the quantum random energy model*, Phys. Rev. B **93**, 024202 (2016), doi:10.1103/PhysRevB.93.024202.
- [67] Y. Huang and B. I. Shklovskii, *Anderson transition in three-dimensional systems with non-Hermitian disorder*, Phys. Rev. B **101**, 014204 (2020), doi:10.1103/PhysRevB.101.014204.
- [68] Y. Huang and B. I. Shklovskii, *Spectral rigidity of non-Hermitian symmetric random matrices near the Anderson transition*, Phys. Rev. B **102**, 064212 (2020), doi:10.1103/PhysRevB.102.064212.
- [69] G. De Tomasi and I. M. Khaymovich, *Non-Hermitian Rosenzweig-Porter random-matrix ensemble: Obstruction to the fractal phase*, Phys. Rev. B **106**, 094204 (2022), doi:10.1103/PhysRevB.106.094204.
- [70] G. D. Tomasi and I. M. Khaymovich, *Non-hermiticity induces localization: good and bad resonances in power-law random banded matrices* (2023), 2302.00015.
- [71] V. E. Kravtsov, I. M. Khaymovich, E. Cuevas and M. Amini, *A random matrix model with localization and ergodic transitions*, New J. Phys. **17**, 122002 (2015), doi:10.1088/1367-2630/17/12/122002.

## A Multifractal spectrum $f(\alpha)$ and fractal dimensions $D_q$

In this Appendix we show the multifractal analysis for the spectrum of fractal dimensions, Figs. 9 and 10, and for the fractal dimensions, Figs. 11 and 12, in the three distinct part of the spectrum, shown in Fig. 8. One can see some deviations from the ergodicity in the delocalized parts (two rightmost rows in all the above figures), that may though be finite-size effects. Therefore in the main text we don't claim any fractality or multifractality of these states, focusing on the localization (leftmost rows) versus delocalization (the rest).

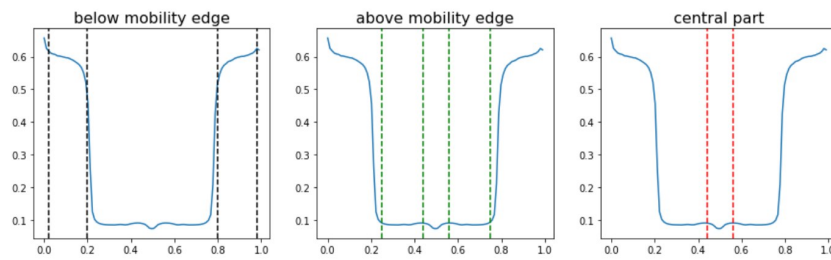


Figure 8: The derivative of IPR versus energy for  $W = 30$  and  $\beta = 0.5$ , used to separate the energy windows for the next four figures: (left) below the mobility edge (localized states),  $|E| > E_{ME1}$ ; (middle) above the mobility edge (delocalized states),  $E_{ME2} \leq |E| \leq E_{ME1}$ ; (right) in the central (not fully ergodic) part,  $|E| < E_{ME2}$ .

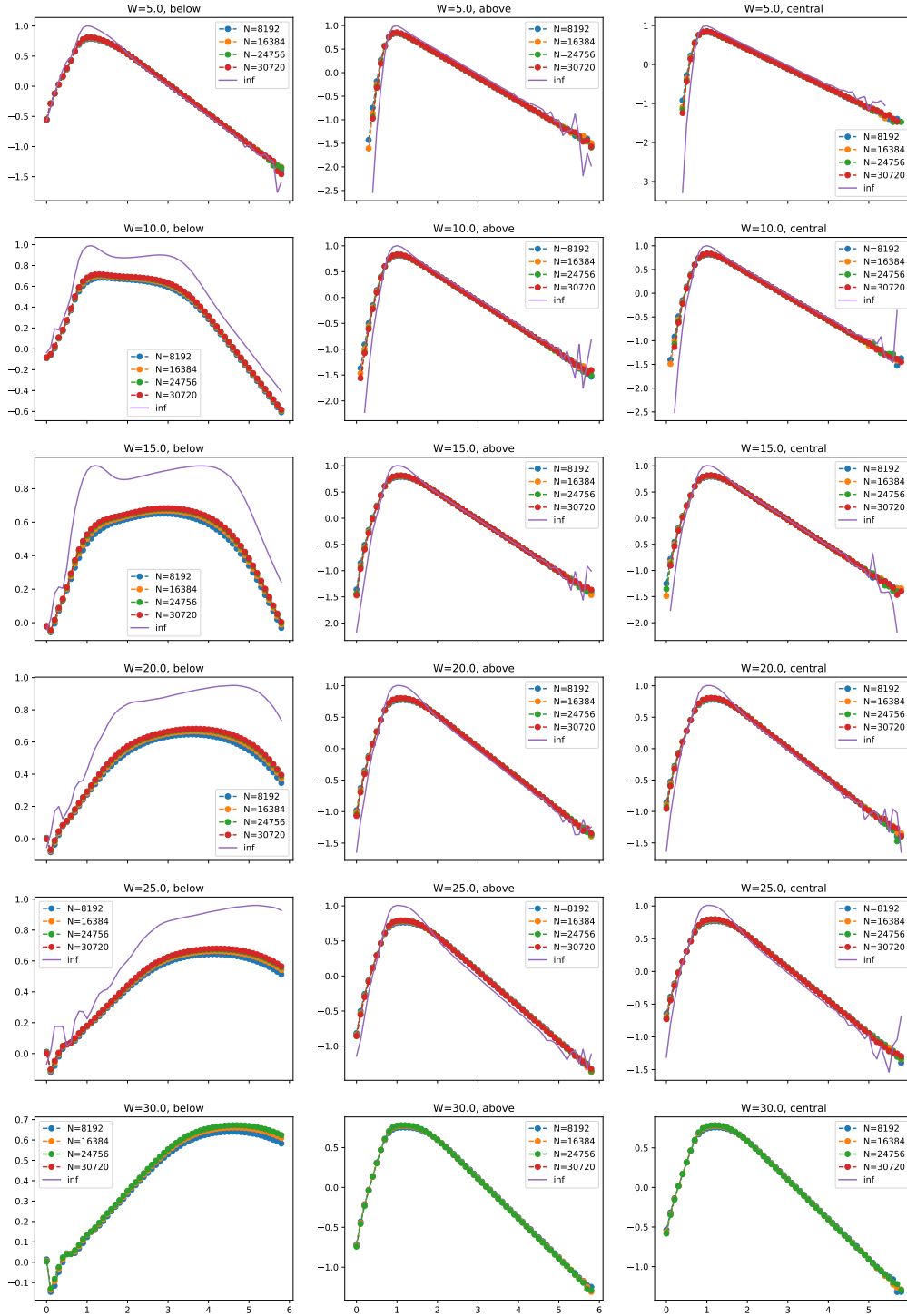


Figure 9: The spectrum of fractal dimensions  $f(\alpha)$  for different disorder amplitudes  $W$  and  $\beta = 0.5$  in different parts of spectrum (see Fig. 8): (left) below the mobility edge (localized states),  $|E| > E_{ME1}$ ; (middle) above the mobility edge (delocalized states),  $E_{ME2} \leq |E| \leq E_{ME1}$ ; (right) in the central (not fully ergodic) part,  $|E| < E_{ME2}$ . Colored symbols show finite-size data, while the solid purple line shows an extrapolated curve [8, 60, 71].

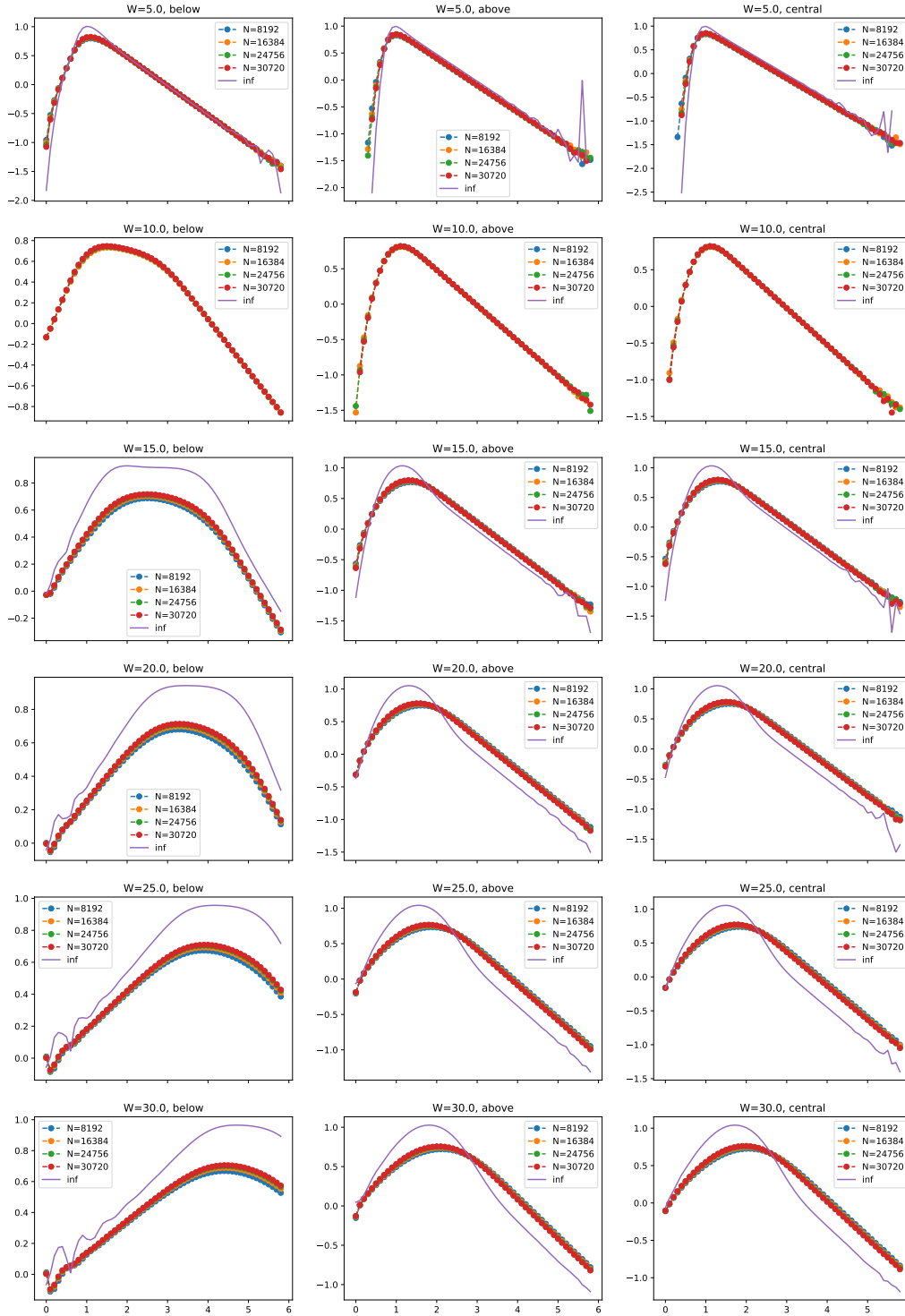


Figure 10: The spectrum of fractal dimensions  $f(\alpha)$  for different disorder amplitudes  $W$  and  $\beta = 0.75$  in different parts of spectrum (see Fig. 8): (left) below the mobility edge (localized states),  $|E| > E_{ME1}$ ; (middle) above the mobility edge (delocalized states),  $E_{ME2} \leq |E| \leq E_{ME1}$ ; (right) in the central (not fully ergodic) part,  $|E| < E_{ME2}$ . Colored symbols show finite-size data, while the solid purple line shows an extrapolated curve [8, 60, 71].

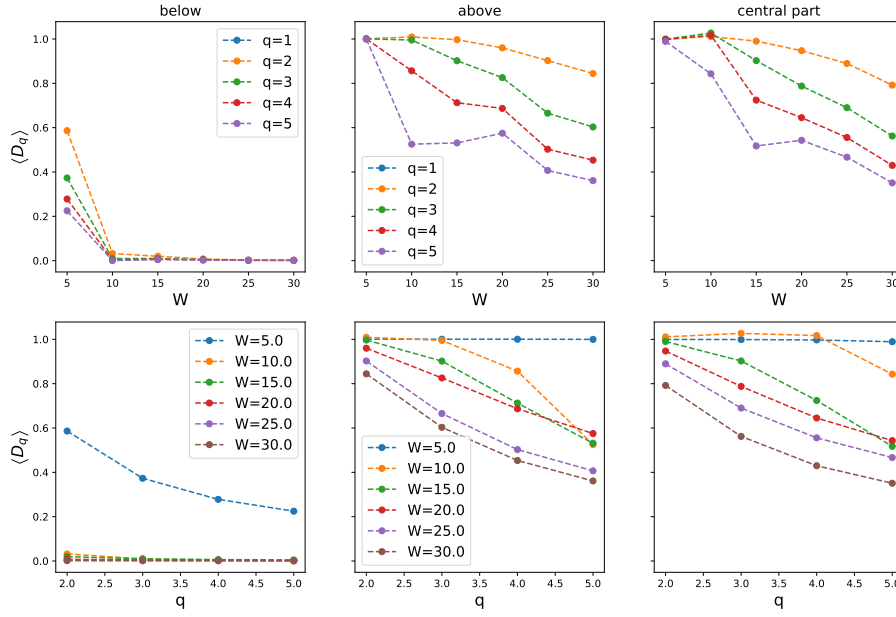


Figure 11: Fractal dimensions  $D_q$ , extrapolated from the finite sizes of Fig. 9, (upper row) versus disorder for different  $q$  and (lower row) versus  $q$  for different disorder amplitudes  $W$  in the partially disordered RRG in different parts of spectrum (see Fig. 8): (left) below the mobility edge (localized states),  $|E| > E_{ME1}$ ; (middle) above the mobility edge (delocalized states),  $E_{ME2} \leq |E| \leq E_{ME1}$ ; (right) in the central (not fully ergodic) part,  $|E| < E_{ME2}$ . The fraction of disordered nodes is  $\beta = 0.5$ .

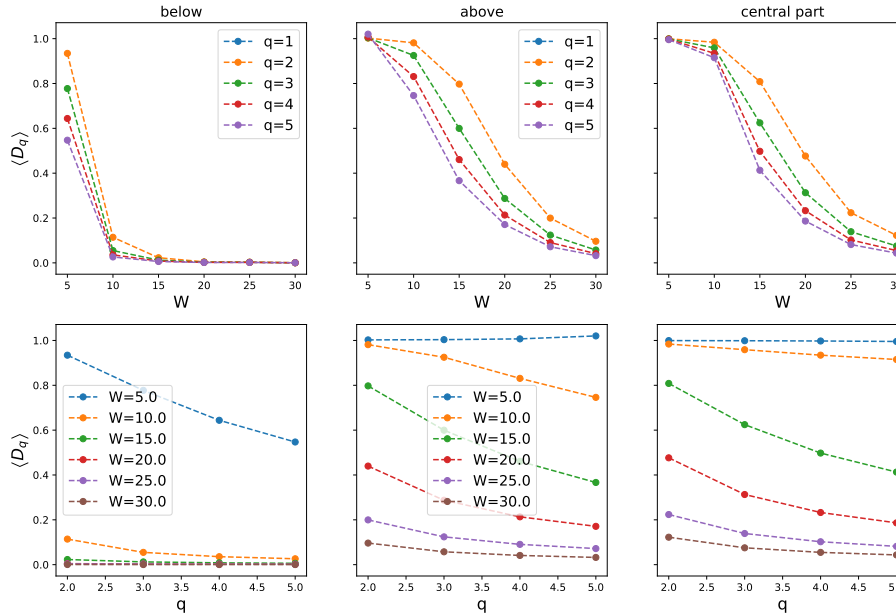


Figure 12: Fractal dimensions  $D_q$ , extrapolated from the finite sizes of Fig. 9, (upper row) versus disorder for different  $q$  and (lower row) versus  $q$  for different disorder amplitudes  $W$  in the partially disordered RRG in different parts of spectrum (see Fig. 8): (left) below the mobility edge (localized states),  $|E| > E_{ME1}$ ; (middle) above the mobility edge (delocalized states),  $E_{ME2} \leq |E| \leq E_{ME1}$ ; (right) in the central (not fully ergodic) part,  $|E| < E_{ME2}$ . The fraction of disordered nodes is  $\beta = 0.75$ .

## B Partial disorder on directed graphs

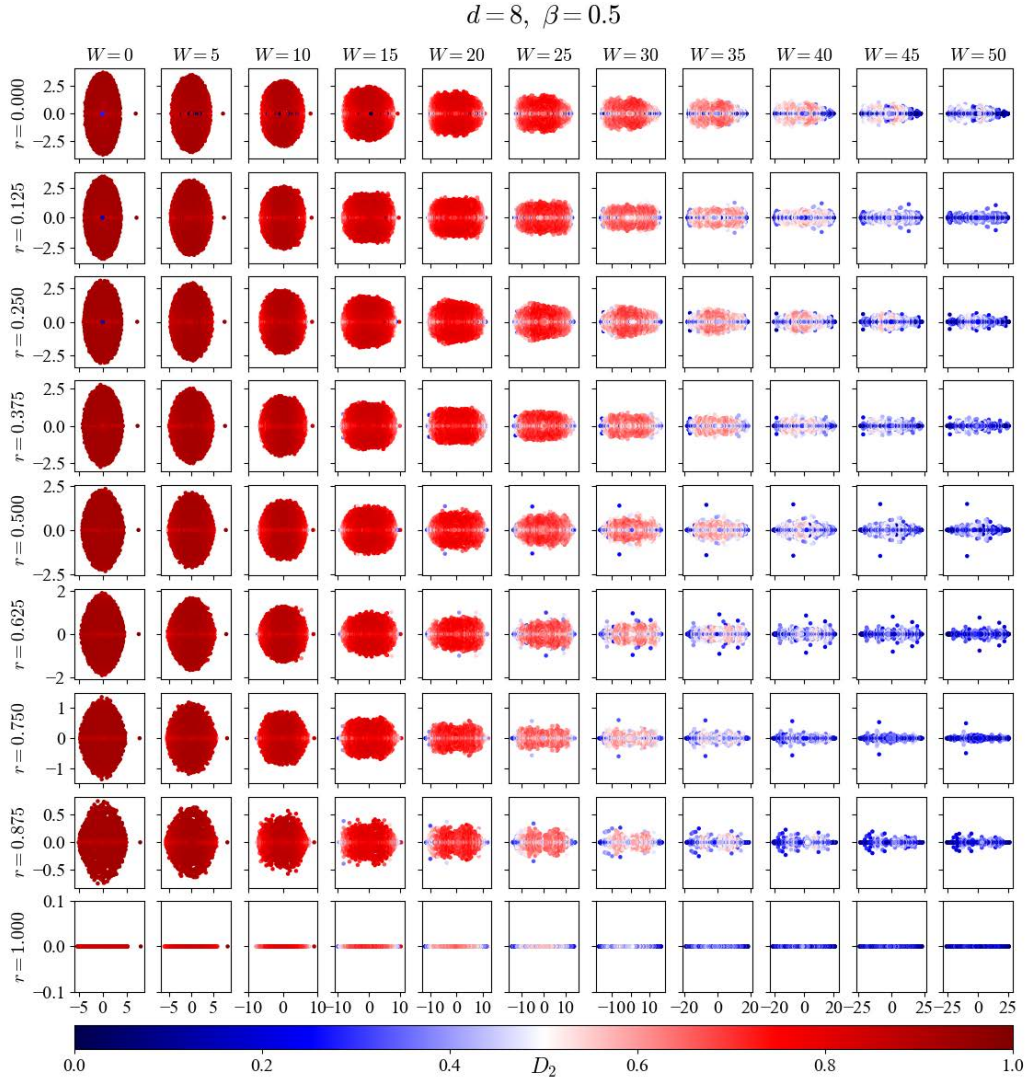


Figure 13: **Complex-valued spectra of the partially disordered and partially non-reciprocal RRG** with the node degree  $d = 8$  for different reciprocity parameters  $r$  and disorder amplitudes  $W$  at the fraction of disordered nodes  $\beta = 0.5$ . Each plot is colored by fractal dimension value  $D_2$ . For all sub-figures, diagonal disorder distribution has the same realization from the interval  $[-1/2; +1/2]$ , but multiplied by  $W$ .

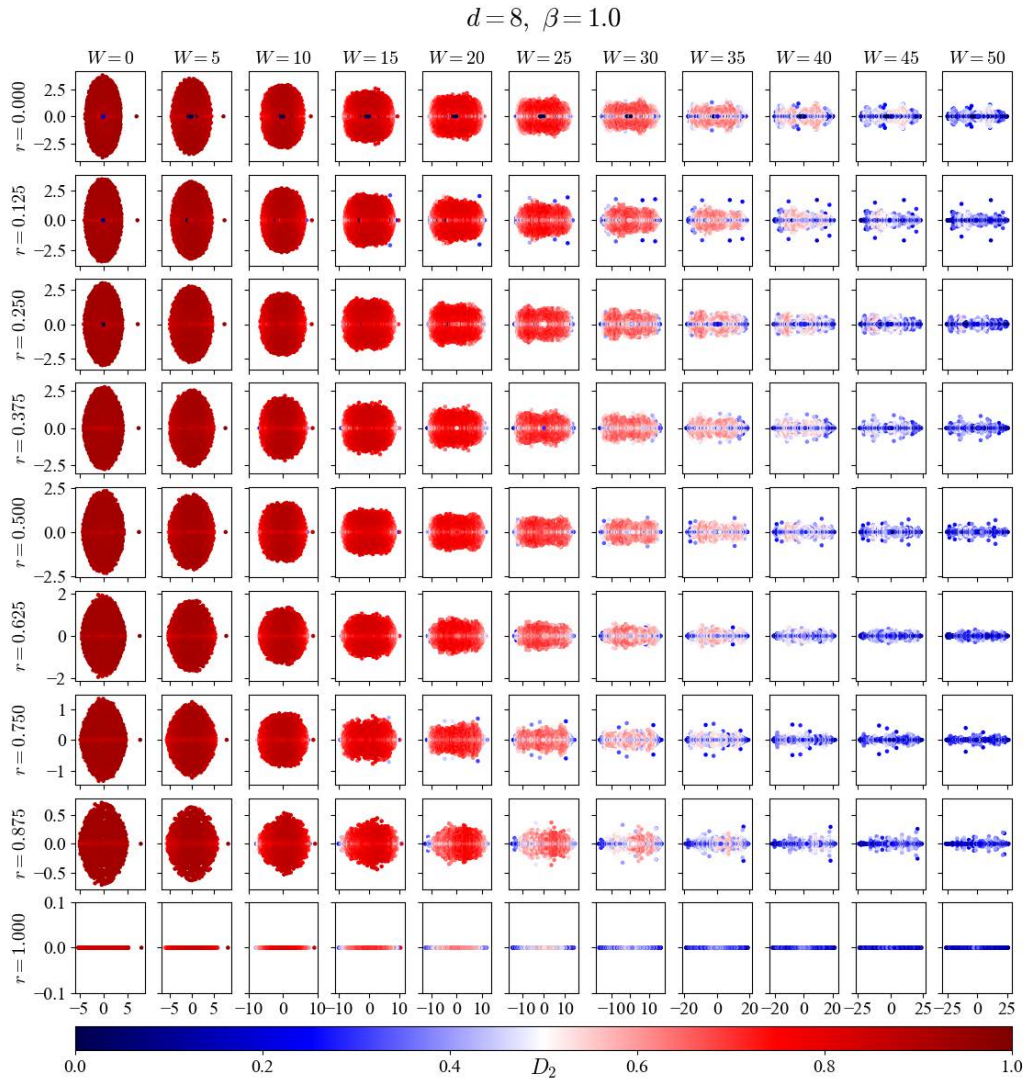


Figure 14: **Complex-valued spectra of the fully disordered ( $\beta = 1$ ) and partially non-reciprocal RRG with the node degree  $d = 8$  for different reciprocity parameters  $r$  and disorder amplitudes  $W$ . Each plot is colored by fractal dimension value  $D_2$ . For all subfigures, diagonal disorder distribution has the same realization from the interval  $[-1/2; +1/2]$ , but multiplied by  $W$ .**